Results in Physics 19 (2020) 103356

Contents lists available at ScienceDirect

Results in Physics

journal homepage: www.elsevier.com/locate/rinp

Optimized strategy to restrain the mid-spatial-frequency surface error in computer-controlled optical surfacing

Longxiang Li[a,b,*], Xingchang Li[a,b], Qiang Cheng[a,b], Ruigang Li[a,b], Weijie Deng[a,b], Xiao Luo[a,b], Feng Zhang[a,b], Donglin Xue[a,b], Xuejun Zhang[a,b,*]

[a] Key Laboratory of Optical System Advanced Manufacturing Technology, Changchun Institute of Optics, Fine Mechanics and Physics, Chinese Academy of Sciences, Changchun 130033, China
[b] Changchun Institute of Optics, Fine Mechanics and Physics, Chinese Academy of Sciences, Changchun, Jilin 130033, China

ARTICLE INFO

Keywords:
Computer-controlled optical surfacing
Lap tool
Dwell-time algorithm
Mid-spatial-frequency surface error
Complete convolution

ABSTRACT

In computer-controlled optical surfacing (CCOS), the paths of the lap tools are limited inside the optical surface; this restricts convolution in the dwell-time algorithm and causes mid-spatial-frequency surface errors. An optimized strategy ensuring relatively complete convolution of the dwell-time algorithm is developed to control the mid-spatial-frequency surface error and simultaneously ensure high optical manufacturing efficiency. Different-sized lap tools are then introduced to correct the surface error in different areas of the optics. Simulations and experiments using a large off-axis SiC mirror demonstrate the validity of the strategy, and it could be widely applied to CCOS in grinding or polishing processes.

Introduction

In modern optical manufacturing technologies, computer-controlled optical surfacing (CCOS) [1,2] technology by different kinds of lap tools still plays a significant role in high-precision aspherical optics, even though some deterministic techniques like Magnetorheological Finishing (MRF) [3–5] or Ion Beam Figuring (IBF) [6–9] are widely applied. The lap tools in CCOS are different from MRF or IBF, and one of the differences is that the tool paths of laps are always limited inside the optical surface; that is, the lap tool cannot move to the very edge of the optical surface to avoid the danger of the laps turning over [10]. This limitation of the tool path, by restricting the convolution in the dwell-time algorithm, usually causes a type of mid-spatial-frequency surface error, especially when a large lap is used to figure the optics. The mid-spatial-frequency residual surface error is a significant obstacle to opticians involved in further improving the precision of optics. Moreover, in many cases, although the peak-to-valley (PV), root mean square (RMS), and roughness meet the requirements, the mid-spatial-frequency surface error reduces the imaging quality in an optical system. Forbes [11] has observed never-ending struggles with mid-spatial frequencies.

In CCOS, the use of different-sized grinding or polishing laps in manufacturing optics is a routine practice [1,12,13]. When small laps are predominantly used to correct the surface error, the time consumption will be increased. In contrast, when large laps are predominantly used, the mid-spatial-frequency results from tool-path limitation become one of the key causes that restrict the accuracy of optics. Therefore, to restrain the mid-spatial-frequency surface error as well as ensure a high manufacturing efficiency, an optimized strategy is developed in this study.

First, the phenomenon and influence of the incomplete convolution in the dwell-time algorithm are analyzed. Then, the complete convolution in the dwell-time algorithm and an optimized strategy to use different-sized laps are introduced in detail. Finally, simulations and experiments are performed to validate the methods and strategy developed in this article.

Incomplete convolution in the dwell-time algorithm for CCOS

Sequential process of CCOS

CCOS is an effective technique in the manufacture of aspherical optics, including grinding and polishing. It is a typical sub-aperture optical manufacturing technology [14,15], which means that the size of the tools is smaller than that of mirrors or lens. Its sequential process is shown in Fig. 1. First, the surface error map of the aspherical optics is tested, and according to this, the manufacturing parameters, such as the tool's size and path, are chosen. Subsequently, the dwell-time

* Corresponding authors.
E-mail addresses: lilx@ciomp.ac.cn (L. Li), zxj@ciomp.ac.cn (X. Zhang).

https://doi.org/10.1016/j.rinp.2020.103356
Received 23 July 2020; Received in revised form 16 August 2020; Accepted 17 August 2020
Available online 13 September 2020
2211-3797/ © 2020 The Author(s). Published by Elsevier B.V. This is an open access article under the CC BY-NC-ND license (http://creativecommons.org/licenses/by-nc-nd/4.0/).

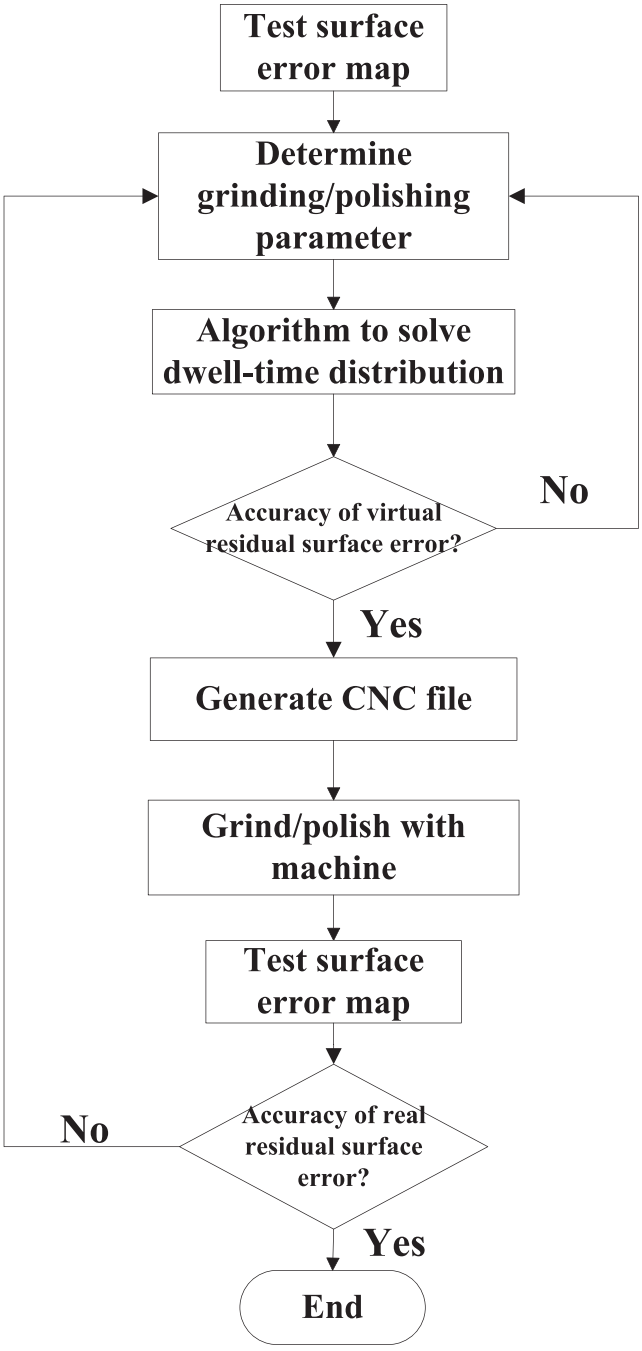

Fig. 1. Sequential process of CCOS.

distribution and virtual residual surface error map are solved by a virtual fabrication via a computer. If the residual surface error is small enough to meet the demands of the optics, the dwell-time distribution map is translated into a CNC file for the CCOS machine for grinding or polishing. Alternatively, the virtual fabrication is repeated to obtain a new dwell-time map by changing the grinding or polishing parameters, until the virtual residual surface error reaches a high level. Finally, the optics enter a loop of testing, virtual and actual fabrication, until the residual surface error satisfies the error criterion.

As shown in the sequential process, the algorithm to solve the dwell-time distribution is a crucial step, as the dwell-time distribution determines the actual residual surface error after grinding or polishing. Usually, the features of the actual surface error map are similar to those of the virtual one [16]. For example, if the mid-spatial frequency is bad in the virtual surface error map, it will not be better in the actual one.

Dwell-time solution algorithm

In CCOS, the key dwell-time distribution is based on the principle that the desired removal amount of material on the optics is a discrete two-dimensional (2D) convolution operation of the dwell time and removal function. As described in Eq. (1), *E(x,y)* is the surface error map before grinding or polishing, which represents the desired material removal on the optical surface. *R(x,y)* is the tool removal function or influence function, which is closely related to the tool's parameters. *T(x,y)* is the dwell time that should be solved. The value of *T(x,y)* is non-negative or positive. According to Eq. (1), the process to obtain the dwell time is a discrete 2D deconvolution in the algebra [17,18], which is represented by the symbol '**':

$$E(x, y) = R(x, y) ** T(x, y) \quad (1)$$

With the development of sub-aperture optical manufacturing technologies, two main kinds of dwell-time algorithms have been established. One is designed to deal with the discrete convolution model directly, such as in the Fourier transform method [9,19], the iterative method, and the series expansion method [20,21]. The other is designed to transform the convolution format into linear matrix equations in algebra, and then solve the linear matrix equations to obtain the dwell-time distribution [8,22,23]. The dwell-time algorithm used in this paper is described in detail in Ref. [16].

Tool path limited inside the optical surface

For the CCOS, the grinding or polishing lap is used to correct the surface error. Usually, this lap tool moves on the optical surface in the grinding or polishing process as shown in Fig. 2(a). In situation A in Fig. 2(a), the lap moves inside the optical surface; in situation B, the lap tool is very near the edge of the optics. If the lap tool moves beyond a certain limit of the edge area, it could turn over and this is unsafe for the optics. Therefore, the lap tool has to be limited within a safe area on the optical surface when the tool path is designed. For comparison, the IBF tool is depicted in Fig. 2(b). Regardless of situation A, B, or C for IBF, the optical surface can be fabricated normally and safely. Therefore, the boundary of the IBF tool path can extend outside the edges of optical parts.

Considering the above, the tool path of CCOS is designed to keep the lap tool working safely and effectively as shown in Fig. 3. *L* represents the distance between the border of the tool path and that of the optical surface. In fact, both the conventional lap tool path and the stressed-lap [24] tool path should be limited inside the optical surface.

Incomplete convolution in the dwell-time algorithm

The limited tool path inside the optical surface leads to no distribution of dwell time in the optical surface edge area. In the dwell-time algorithm, this introduces a kind of mid-spatial-frequency residual surface error, which is similar to the ring effect in image restoration, although it is not identical [17]. This mid-spatial-frequency surface error is an oscillation similar to a water wave. If the size of the lap tool is small compared to that of the optical surface, the oscillation is concentrated in the edge region. However, when the relative size of the lap tool is large, the oscillation is distributed over the whole residual surface error map, for example, as shown in Fig. 4(b). The spatial period of this type of mid-spatial frequency is similar to the size of the removal function area from lap tool. The corresponding tool removal function is shown in Fig. 4(a).

As mentioned in Section 2.2, in the dwell-time algorithm, the convolution of the removal function and dwell time is equal to the distribution of desired material removal. If a tool such as MRF or IBF can extend beyond the optical parts along the planned path, a relatively complete convolution happens between the removal function and dwell time, and the mid-spatial-frequency surface error mentioned above will

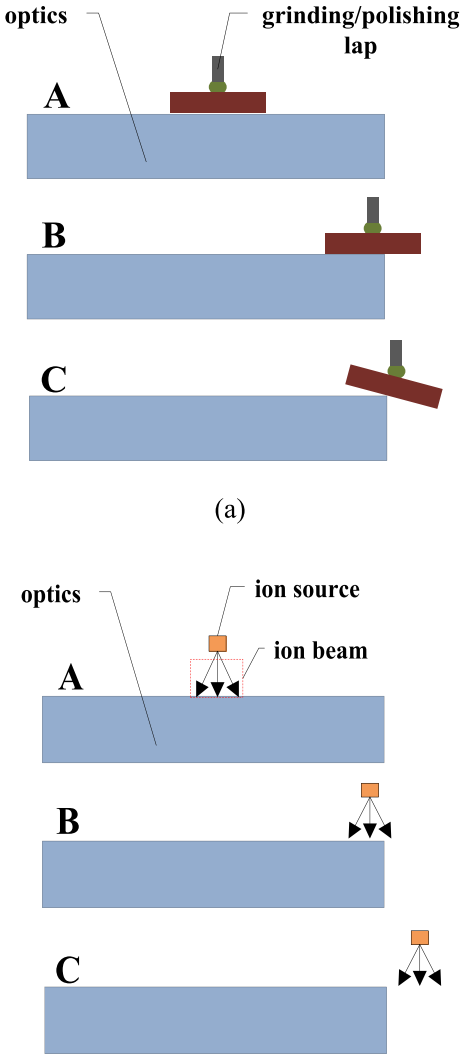

Fig. 2. Tools on an optical surface in the fabricating process: (a) conventional lap tool, (b) IBF tool.

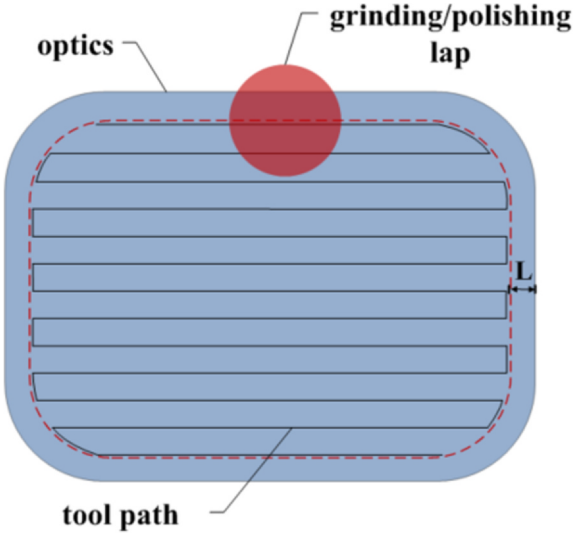

Fig. 3. Tool path for the grinding or polishing lap in CCOS.

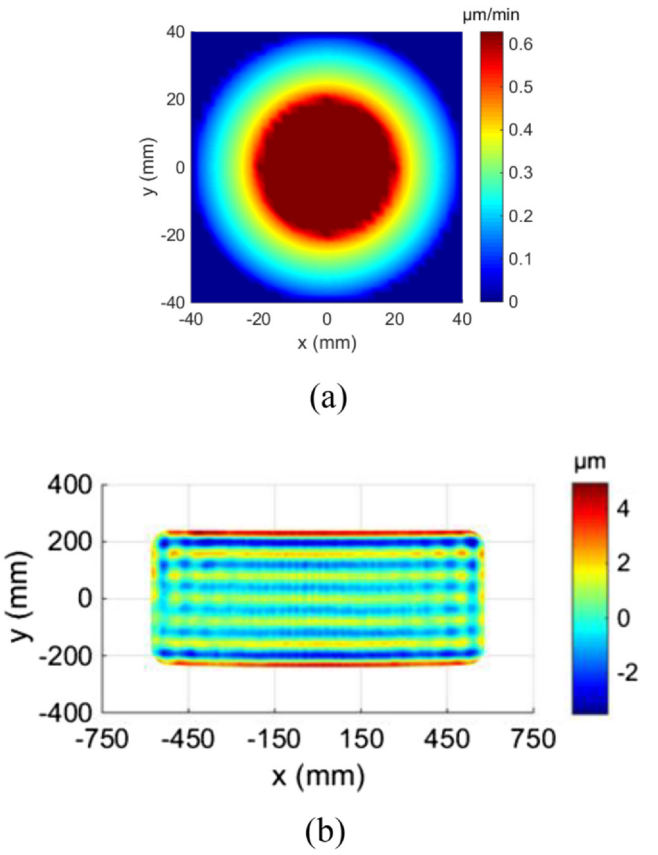

Fig. 4. Oscillation of the virtual residual surface error map by lap tool: (a) removal function, (b) virtual residual surface error map.

be small. Comparatively, if a lap tool path is limited inside the optical surface, a relatively incomplete convolution compared to the MRF or IBF occurs in the dwell-time algorithm and the mid-spatial-frequency surface error mentioned above is large.

Optimized combination strategy to restrain the mid-spatial-frequency surface error resulting from incomplete convolution

Virtual complete convolution in the dwell-time algorithm for the lap tool

In this section, a method is proposed to restrain the mid-spatial-frequency surface error resulting from incomplete convolution in the dwell-time algorithm.

First, without considering working safely, a lap tool path in CCOS is planned in the same manner as IBF or MRF whose tool can extend outside the optical parts, as shown in Fig. 5. This kind of tool path, of course, cannot be used to correct the surface error directly. However, the mid-spatial-frequency residual surface error from solving the dwell-time map by deconvolution simulation, according to the initial surface error map and removal function by a large lap tool, is controlled to be weak. The dwell-time map of the full aperture, some of which is outside the optics, is obtained. This is shown in Fig. 6. The lap tool size is chosen to be large as it is necessary to consider higher manufacturing efficiency for optics.

Second, to ensure that the dwell-time map is suitable for the actual grinding or polishing process, the safe tool path constraints to avoid the lap's overturning in the edge area of the optics should not be ignored. With the safe tool path constraints, the dwell-time map of the full-aperture tool path in the first step above is divided into two parts. One part is that in which the dwell-time of the path is limited within the safe area on the optical surface, as shown in Fig. 2(a), and the safe area path is similar to that in Fig. 3. This part is used in the actual grinding or

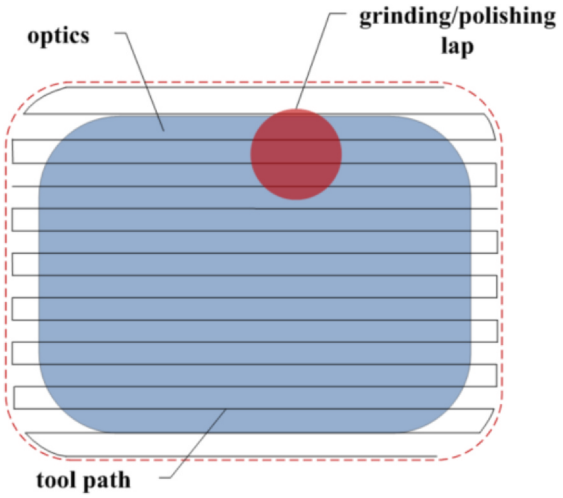

Fig. 5. Lap tool path planned in CCOS, which stretches outside the optical parts.

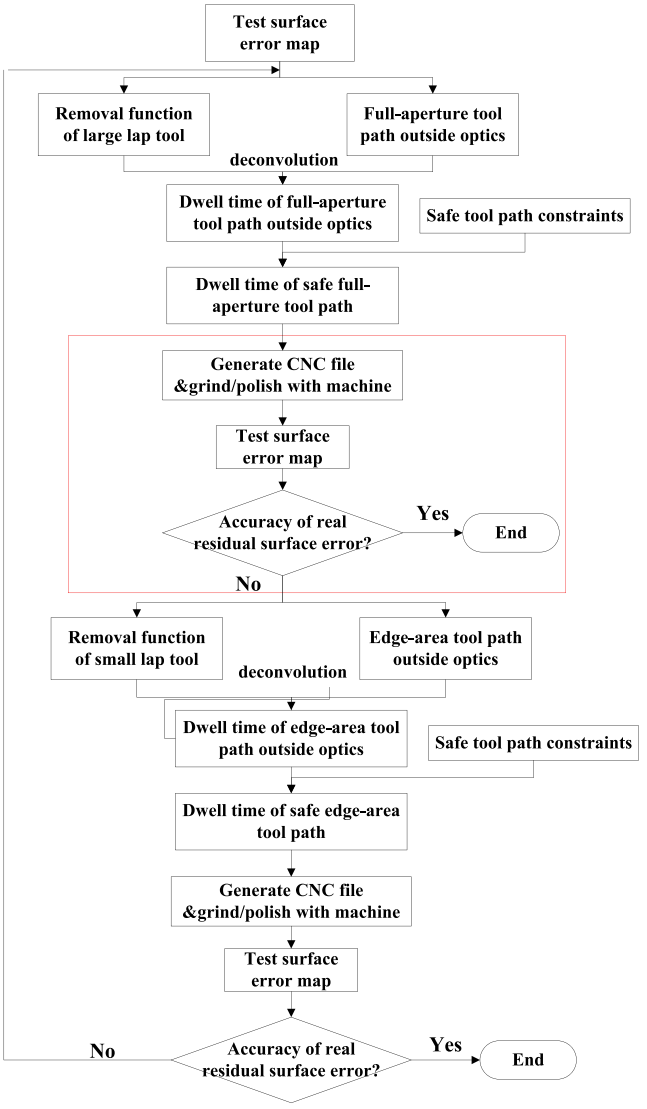

Fig. 6. Optimized combination strategy to restrain the mid-spatial-frequency surface error resulting from incomplete convolution in CCOS.

polishing process. The other part of the full-aperture dwell-time map is abandoned.

It should be noted that while only one part of the dwell-time map is used, the surface error cannot be corrected fully as predicted by the virtual result from the deconvolution in the dwell-time algorithm based on the tool path extending outside the optics. The inner part of the full-aperture optical surface error is corrected in the right way and the mid-spatial frequency in this inner area is restrained to a very weak level. This will be proven in the next section by simulations and experiments. The opposite of the inner part is the edge-area surface error, which is not corrected in the right way. Because the dwell-time map that is excluded in the safe tool path is abandoned, the residual surface error in the edge area is usually distributed at a high level.

Combination of different-sized lap tools

As analyzed above, the edge-area residual surface error also needs to be corrected fully to satisfy the accuracy requirements of the optics. An effective method of using a smaller lap tool to control the edge-area residual surface error is introduced and described below.

By considering higher manufacturing efficiency for optics, the smaller lap tool, compared to the large lap tool mentioned in Section 3.1, is used to correct the surface error only within the edge area, even though the smaller lap tool can be used for the full aperture.

Firstly, for the small lap tool, the path is planned as shown in Fig. 7(a), which also extends outside the optics. The dwell time of the edge-area tool path outside the optics is solved by deconvolution between the removal function of the small lap and the surface error map, which is the residual surface error after being corrected by the large lap tool in the previous process, as shown in Fig. 6.

This type of dwell-time map, just like that of the large lap tool, cannot be directly used to correct the surface error in the actual process. It is also divided into two parts. One part is that in which the dwell time of the path is limited within the safe area on the optical surface, and the safe edge-area tool path is shown in Fig. 7(b). *L'* represents the distance between the border of the safe tool path and that of the optical surface. The other part, which causes the lap to turn over, is abandoned. The dwell time of the safe edge-area tool path is then used to generate the CNC file that is used in the actual grinding or polishing process, as shown in Fig. 6.

After using the small lap tool, the surface error is tested again. If the optical surface accuracy in the clear aperture satisfies the requirements, the correcting process is terminated. Alternatively, the strategy in Fig. 6 is repeated with a different-sized lap tool and other changed parameters.

Some necessary discussions

(a) The mid-spatial-frequency surface error resulting from incomplete convolution of the dwell-time algorithm in CCOS, as shown in Fig. 4(b), is restrained by the strategy introduced in sections 3.1 and 3.2. This will be proven by simulations and experiments in the following section. One can, of course, choose a very small lap tool to correct the full-aperture surface error and the mid-spatial-frequency error from the small lap can be predicted to be not strong. However, in the project-use optics, the time consumption is always a crucial factor that opticians have to consider seriously. The strategy in this paper provides an opportunity for the large lap tool to be used in applications while the mid-spatial-frequency surface error is restrained to be very weak. That is to say, this strategy ensures the high manufacturing efficiency of optics while simultaneously improving accuracy.

(b) After the combination of the large and small lap tools in correcting the surface error in the strategy above, the inadequate-correcting surface error is compressed within a small area near the edge of the optics. The size of the small lap should be chosen according to the

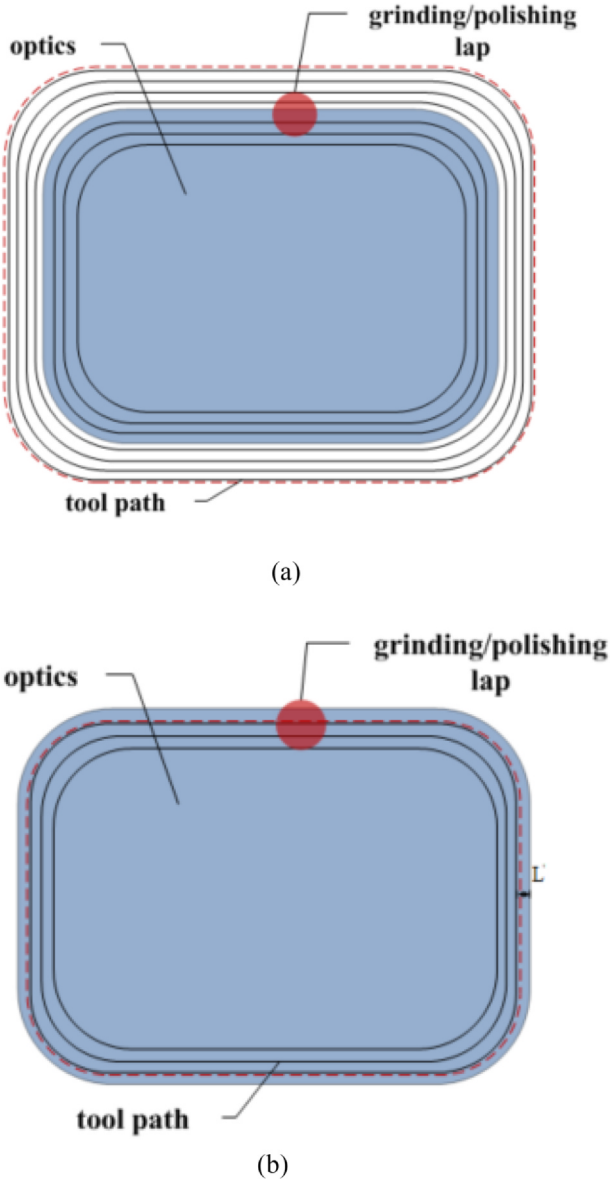

Fig. 7. Tool path for small lap tool: (a) edge-area tool path outside optics, (b) safe edge-area tool path.

size of the clear aperture and full aperture of the optics so that the inadequate-correcting surface error can be compressed outside the clear aperture, increasing the accuracy of the clear aperture up to a high level. Furthermore, a reasonable edge-effect-influenced removal function can be studied and used to control the inadequate-correcting residual surface error after the use of the small lap.

(c) The procedure shown in Fig. 6 can be flexibly and smartly applied in the actual manufacturing process. For example, the large lap's steps of "Generate CNC file and grind/polish with machine" and "Test surface error map", which are marked by the red border in Fig. 6, can be omitted properly. This means the deconvolution to solve the dwell time for the small lap would be based on the simulated residual surface error map from deconvolution for the large lap tool on the optics. Therefore, a different-sized lap tool could be used to correct the surface error after only one iteration of testing. Thus, the time consumption of each testing process is reduced. Meanwhile, the edge-effect-influenced removal function and the determinacy of the grinding or polishing should be considered.

In a brief summary, for the strategy proposed in this section. First, for large lap tool, solving the dwell-time map by 'complete convolution' in algorithm, and the truncated dwell-time map by considering safety is used in real process. After figuring by large lap tool, the MSF inside mirrors is retrained. Then, the small lap tool is used to figure the surface error in the edge area of mirrors and its dwell-time map is also solved by 'complete convolution' in algorithm. After using the large and small lap tool, the specific MSF is controlled in the clear aperture of mirrors.

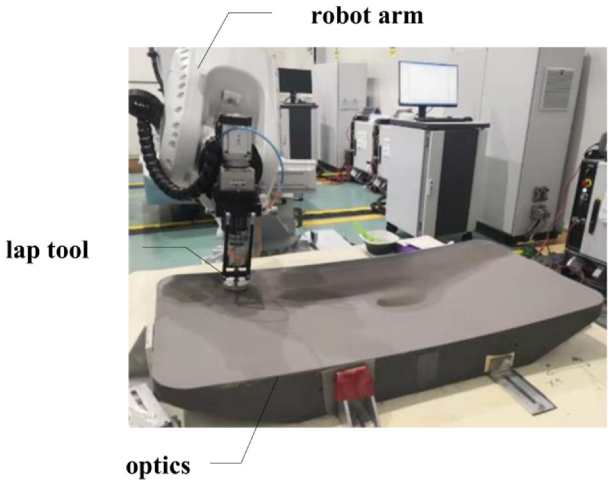

Fig. 8. Experimental set-up: a lap tool is integrated into a robot arm.

Simulations and experiments

Description of simulation and experiment conditions

To prove the validity of the optimized combination strategy introduced above, simulations and experiments are conducted based on an aspherical mirror. The experimental set-up comprises a robot arm into which the lap tool is integrated, as shown in Fig. 8. The related optical manufacturing software is developed. The mirror is an off-axis aspherical mirror consisting of RB-SiC material. The size of the mirror is approximately 1400 mm × 600 mm. The simulations and experiments are conducted during the grinding process of the mirror, according to the strategy introduced in section 3 and shown in Fig. 6. The initial surface error map of the simulations and experiments is shown in Fig. 9(a), in which the values of PV and RMS are 34.75 μm and 4.4 μm, respectively. The diamond abrasive is used in the grinding process to remove the SiC material.

Large lap tool correcting full-aperture surface error

The diameter of a large lap tool under planar motion mode is 60 mm with an eccentric distance of 10 mm, and the corresponding removal function is shown in Fig. 4(a). The tool's rotation velocity is 300 rpm and the tool's pressure is 2 atm. The tool path is planned outside the mirror as shown in Fig. 5, and the distance of the path from the border of the mirror is at least half of the influenced area of the removal function. The distance in this simulation is 40 mm, which is just half of the 80-mm influenced area of the removal function shown in Fig. 4(a). The dwell point interval for this lap tool is set to 10 mm.

Subsequently, the deconvolution happens between the initial surface error and the removal function to obtain the dwell-time map by simulation. The dwell-time map of the full aperture, 40 mm of which is outside the optics, is shown in Fig. 9(b), in which the black dotted line is the border of the full aperture of the mirror. As mentioned above, this kind of full-aperture dwell-time map cannot be used to correct the surface error in reality. Therefore, the safe tool path constraints must be considered and the dwell-time map of a safe full-aperture tool path is obtained, as shown in Fig. 9(d) according to the path shown in Fig. 3.

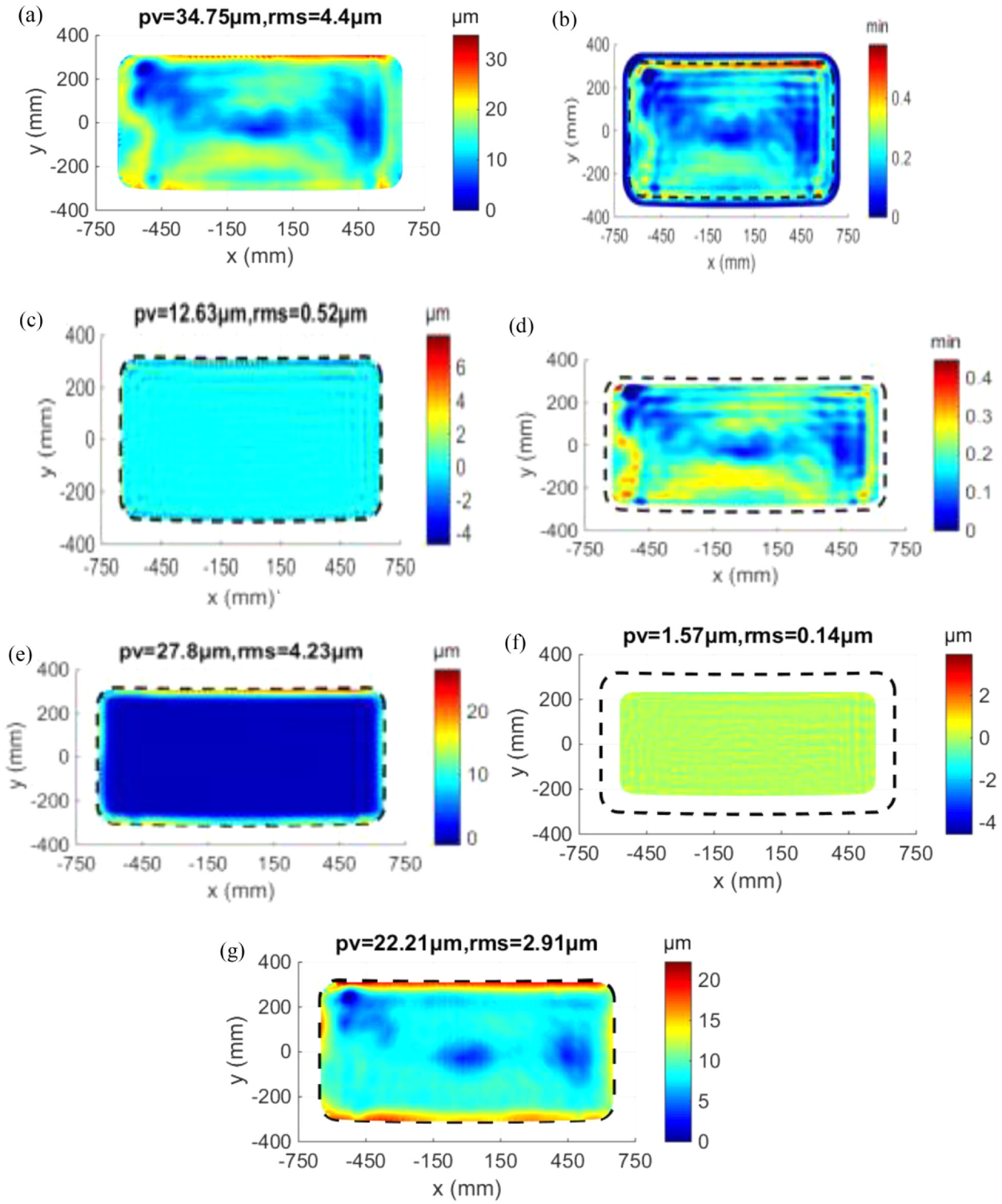

Fig. 9. Simulation and experiment of a SiC off-axis aspherical mirror using a large lap tool: (a) initial surface error map, (b) dwell time of the full-aperture tool path outside the optics, (c) virtual residual surface error by the large lap, (d) dwell-time map of the safe full aperture, (e) virtual residual surface error according to the dwell-time map of the safe full aperture, (f) virtual residual surface error in the inner part of the full-aperture optics, (g) real residual surface error after grinding.

The distance of the safe full-aperture tool path from the border of the mirror, which is L in Fig. 3, is chosen as 30 mm in this simulation and experiment. The dwell-time map of the safe full-aperture tool path would be used in the actual grinding process, and the corresponding virtual residual surface error is shown in Fig. 9(e). As the dwell time outside the safe area on the optical surface is abandoned, the virtual residual surface error in Fig. 9(e) indicates that the surface error in the edge-area near the border of the optics is not fully corrected. However, the inner part of the full-aperture optical surface error is corrected, and the mid-spatial-frequency error is restrained to be very weak, as shown in Fig. 9(f). In order to have a contrast, the color-bar of Fig. 9(f) is adjusted to be the same with that of Fig. 11 (b). The distance from the mirror's border, which is marked by the black dotted line in Fig. 9(f), to the border of the inner part of the full-aperture optical surface error is

the diameter of the removal function, which is 80 mm in this simulation.

Next, the CNC file is generated according to the dwell-time map of the safe full-aperture tool path, as shown in Fig. 9(d). The CNC file is executed by the machine to grind the mirror, as shown in Fig. 8. In reality, to avoid project risks, the dwell-time map is usually not conducted to a 100% degree. In this experiment, an approximately 40% degree of dwell time is conducted, which means that only 40% of the dwell-time value at each dwell point on tool path is used to generate the CNC file.

After the actual grinding, the real residual surface error is shown in Fig. 9(g), and the values of PV and RMS are found to be 22.21 μm and 2.91 μm, respectively. The values of PV and RMS are both reduced, compared to those of the initial surface error. The mid-spatial-frequency surface error, which is an oscillation similar to a water wave, does not appear in the inner part of the full aperture, although the surface error in the edge-area near the border of the optics is not fully corrected, as predicted in the simulation above. This proves the validity of the method of using the large lap tool to correct the full-aperture error, while restraining the mid-spatial-frequency surface error in the inner part by the complete convolution in the dwell-time algorithm.

One more point that requires explanation is that the values of PV and RMS of the real residual surface error are smaller than those of the virtual residual surface error. There are two reasons for this. The first is that the material removal rate and its distribution in the removal function by the lap tool deviated from the actual one, and the removal function used in this experiment is from a simulated model by experience. Of course, the removal function of the lap tool with abrasives is influenced by many parameters and these parameters are usually not constant or uncontrollable, which is one of the reasons that the lap tool lacks determinacy compared with IBF or MRF. The other reason is that the change of the removal function in the edge area of the optics is not considered thoroughly; the real residual surface error in the edge area is somewhat different from the simulated one.

Small lap tool correcting edge-area surface error

Firstly, the diameter of the small lap tool in planar motion is chosen to be 20 mm with an eccentric distance of 5 mm. The corresponding removal function is shown in Fig. 10 (a). The tool's rotation velocity is 200 rpm and the pressure is 0.6 atm. The dwell point interval for this lap tool is set to 4 mm. The initial surface error map for the small lap tool is just the real residual surface after grinding by the large lap, as shown in Fig. 9(g). The tool path is planned as shown in Fig. 7(a). It stretches outside the mirror and the distance from the border of the mirror is at least half the size of the removal function of the small lap, as with the large lap. Therefore, this distance outside the mirror is 15 mm. By considering higher manufacturing efficiency for optics, the tool path for the small lap tool does not cover the inner part of the mirror, as shown in Fig. 7(a), and the distance from this inner part to the border of the mirror is 70 mm. The 70 mm distance consists of two parts: 30 mm is just the safe distance for the large lap L in Fig. 3; the other 40 mm is half the size of the large lap's removal function. Indeed, the distance can also be chosen according to the real residual surface error of the large lap tool in the edge-area of the mirror.

Subsequently, the deconvolution happens between the initial surface error, as shown in Fig. 9(g), and the removal function of the small lap, as shown in Fig. 10(a), to obtain the dwell-time map by simulation. The dwell time of the edge-area tool path outside the optics is shown in Fig. 10(b), in which the black dotted line is the border of the aperture of the mirror. The corresponding virtual residual surface error is shown in Fig. 10(c). As mentioned above, this kind of dwell-time map extending outside the surface of the mirror cannot be used to correct the surface error in reality. Taking safe tool path constraints into account, the dwell-time map of a safe edge-area tool path is obtained in Fig. 10(d). The safe edge-area dwell-time map would be used in the actual grinding process, and the corresponding virtual residual surface error is shown in Fig. 10(e), indicating that the inadequate-correcting surface error is compressed within a smaller area near the edge of the optics in the simulation. It is worth noting that a reasonable edge-effect-influenced removal function can be used to control the inadequate-correcting residual surface error, even though this experiment does not include this.

Next, the CNC file is generated according to the safe edge-area dwell-time map, as shown in Fig. 10(d). The CNC file is executed by a 60% degree to grind the mirror. The real residual surface error by the small lap is shown in Fig. 10(f), and the values of PV and RMS are 13.68 μm and 1.94 μm, respectively. The distribution of the real residual surface error is similar to that of the simulated results. These prove the validity of correcting the edge-area surface error with a small lap tool.

Compared simulation

To further prove that the mid-spatial-frequency surface error is restrained effectively, a compared simulation is conducted. In this simulation, a conventional method is applied to the initial surface error, as shown in Fig. 9(a). Only the lap with diameter 60 mm is used, and the tool path is directly planned as shown in Fig. 3 by considering the safe constraints. The deconvolution is executed to solve the dwell time, and this is an incomplete convolution in the algorithm as discussed above. The corresponding virtual full-aperture residual surface error is shown in Fig. 11(a), and the virtual sub-aperture residual surface error is shown in Fig. 11(b), in which the black dotted line is the border of the aperture of the mirror. Comparing the virtual full-aperture residual surface error of the complete convolution in the algorithm shown in Fig. 9(e), with that of the incomplete convolution shown in Fig. 11(a), the PV value of the complete one is a little smaller than that of the incomplete one, but the RMS value of the complete one is noticeably larger. This mainly results from the fact that the dwell-time map from the complete convolution outside the safe area on the mirror is abandoned, and the surface error in the edge-area near the border of the optics is not fully corrected. However, regarding the inner part of the full-aperture optical surface error, the values of PV and RMS of the complete convolution are much smaller than those of the incomplete one.

In order to justify the mid-spatial frequency clearly and quantitatively, the power spectral density(PSD) in one dimension is used as a diagnostic tool. For surface error map of the rectangle mirror in above figures, the coordinate of the data line for 1 D PSD is $x = 0$, for example, red dotted straight line in Fig. 11(b). As shown in Figs. 12, 1 D PSD curve of initial surface error map in Fig. 9(a), virtual residual surface error map by strategy proposed in this paper in Fig. 9(f), compared virtual residual surface error map in Fig. 11(b) and real residual surface error map after figuring in Fig. 10(f), is drawn. The four PSD curves are normalized based on the PSD of the initial surface error map.

For the simulated virtual residual surface error, the compared one by the conventional method as shown in Fig. 11(b) has a typical spatial period as shown in Fig. 12 and the frequency is about 0.0156 mm^{-1} with corresponding spatial period is about 64 mm. The virtual one by the strategy proposed in section 3 as shown in Fig. 9(f), has a spatial period at frequency of 0.0195 mm^{-1} with corresponding spatial period is about 51 mm, whose magnitude of PSD is smaller than that of compared one. This proves that strategy of complete convolution introduced in this article is validated to restrain the mid-spatial-frequency surface error in simulation.

As to the real surface error map, the distribution of PSD curves of the initial surface error and real residual surface error map, is basically consistent. The low-spatial frequency of the real residual surface error is smaller than that of initial surface error at spatial period larger than about 20 mm, which proves that the low-spatial frequency is converged in real fabrication process.

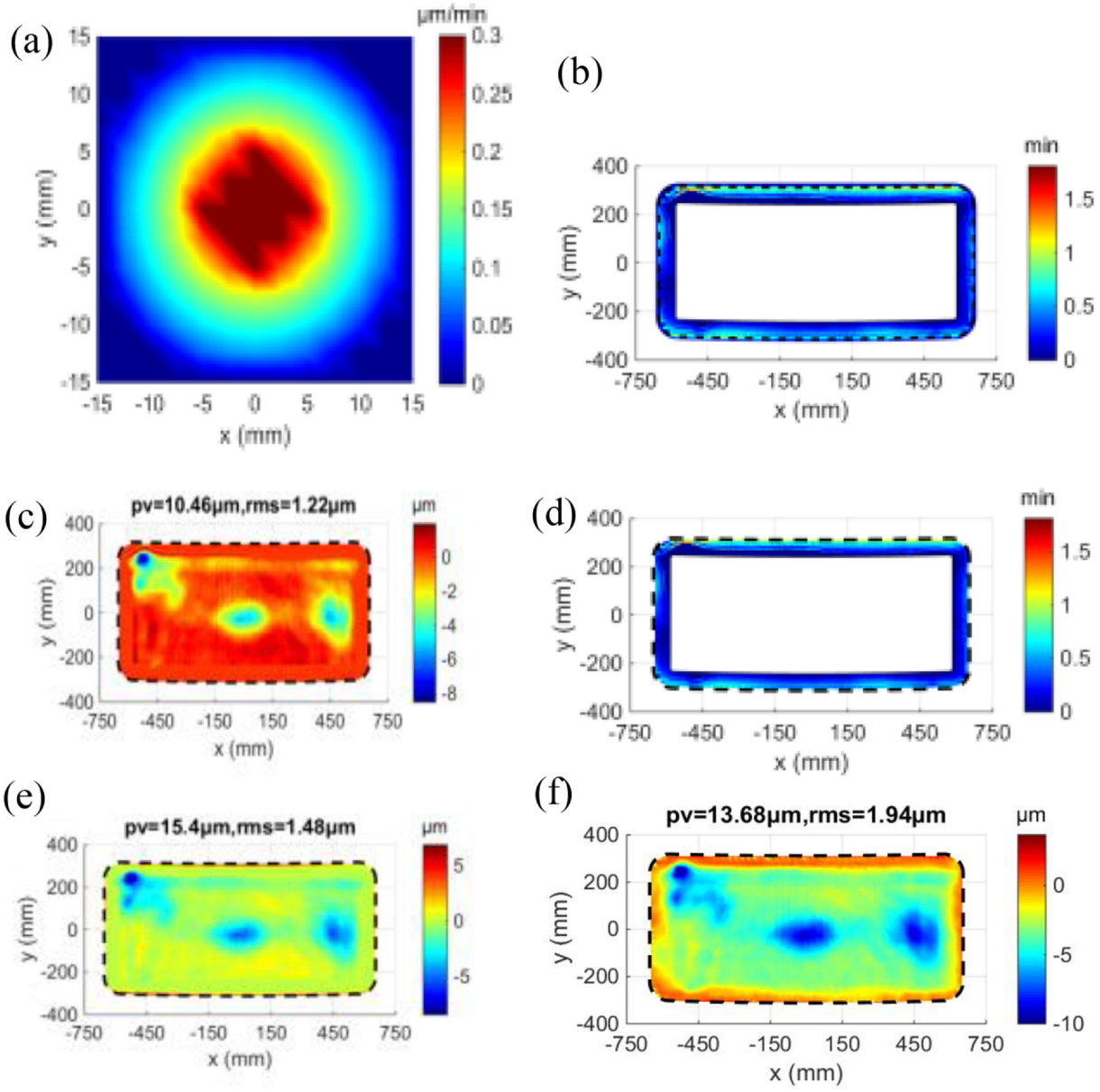

Fig. 10. Simulation and experiment of a SiC off-axis aspherical mirror using a small lap tool: (a) removal function, (b) dwell time of the edge-area tool path outside the optics, (c) virtual residual surface error according to the dwell time of the edge-area tool path outside the optics, (d) dwell-time map of the safe edge-area tool path, (e) virtual residual surface error according to the dwell-time map of the safe edge-area tool path, (f) real residual surface error.

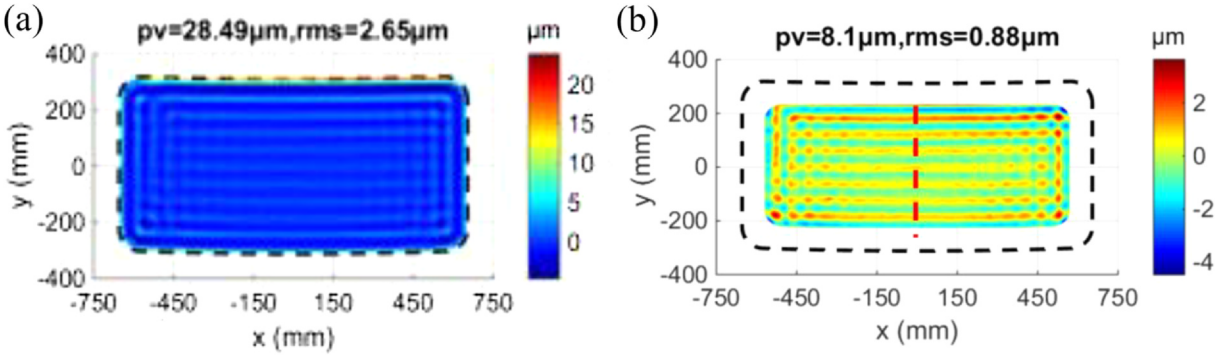

Fig. 11. Compared simulation results of the large lap tool: (a) virtual full-aperture residual surface error map, (b) virtual sub-aperture residual surface error map.

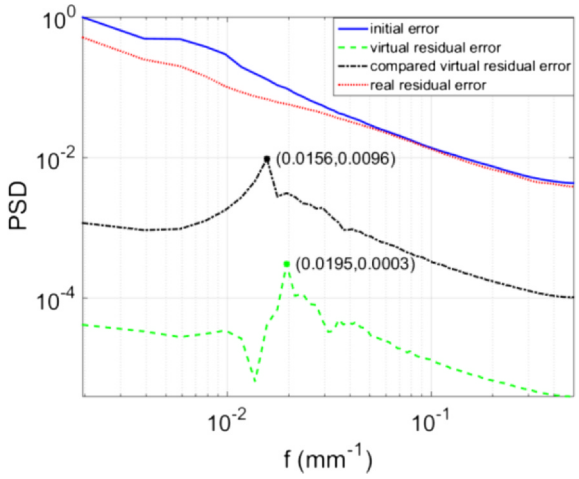

Fig. 12. PSD curve of the surface error map.

Therefore, from simulation, experiments and PSD analysis, the method of complete convolution introduced in this article is validated for restraining the mid-spatial-frequency surface error as well as controlling the PV and RMS of surface error map.

Additional simulation

In order to further prove that middle-spatial-frequency error is created by the incomplete convolution but not by the dwell point interval, an additional simulation is carried on. In this additional simulation, the initial surface error and the size of lap tool are same with those in above compared simulation whose results are shown in Fig. 11, but the dwell point sampling interval is set to be different values. The dwell points sampling interval is 1 mm and 5 mm in this simulation, compared with 10 mm in section 4.4.

The results of the additional simulations are shown in Fig. 13. In Fig. 13(a) and (b) the dwell point sampling interval is 5 mm and in Fig. 13(c) and (d) the dwell point sampling interval is 1 mm. The values of PV and RMS of residual surface error maps with 1 mm and 5 mm dwell point sampling interval in Fig. 13, are similar to those of compared simulation in Fig. 11 in section 4.4. More importantly, the specific mid-spatial frequency is also clear and obvious, which is very similar to that in the results shown in Fig. 11. This proves that the specific mid-spatial frequency is not caused by the dwell point interval. It is worth noting that no matter what type of path is used, for example raster path scanning along x-axis or y-axis, or the random path, once the dwell points are all limited inside a safe area of the optical surface, this kind of middle-spatial-frequency would also exist in the residual surface error map. It is definitely created by the incomplete convolution as mentioned above.

Discussion

The details of simulations and experiments to correct the surface error of a large SiC mirror are introduced above. The PV and RMS converge from initial values of 34.75 μm and 4.4 μm to 13.68 μm and 1.94 μm, respectively. The mid-spatial-frequency surface error resulting from incomplete convolution of the dwell-time algorithm in CCOS is effectively restrained, and in addition, the time consumption is controlled because the large lap tool is still used in the grinding process. The results of the residual surface error, as shown in Fig. 10(f), are favorable for the post-grinding or post-polishing process of the mirror. Moreover, some necessary values of the sizes of the lap tools and corresponding tool paths are introduced in detail, and all these values are references for mirror manufacturing processes. These should be used flexibly and smartly in application for different aspherical optics. In

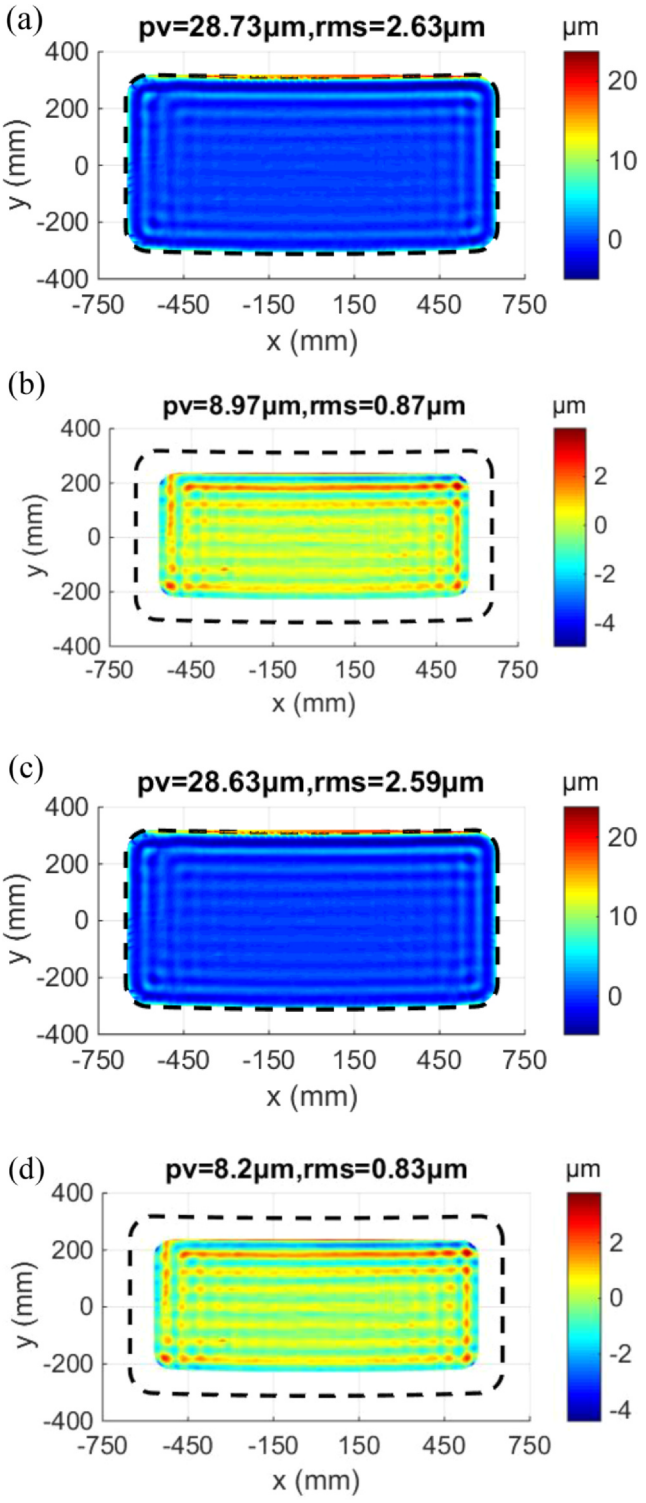

Fig. 13. Additional simulation results of the large lap tool: (a) virtual full-aperture residual surface error map by 5 mm dwell point interval, (b) virtual sub-aperture residual surface error map by 5 mm dwell point interval, (c) virtual full-aperture residual surface error map by 1 mm dwell point interval, (d) virtual sub-aperture residual surface error map by 1 mm dwell point interval.

addition, a more accurate removal function of the lap tool on an aspherical surface or its edge area needs to be considered, and the determinacy of the lap tool may also be improved to accelerate the process of manufacturing aspherical optics. In summary, the simulations and experiments proved the validity of the optimized combination strategy in this article, ensuring high manufacturing efficiency of the optics while simultaneously improving surface accuracy.

Conclusions

In CCOS, when the tool path is limited inside the optical surface to avoid the overturning of the lap, the mid-spatial-frequency error resulting from incomplete convolution of the dwell-time algorithm becomes apparent in the residual surface error map. An optimized strategy to restrain this mid-spatial frequency is introduced and its details are described. Firstly, a relatively complete convolution of the dwell-time algorithm is built by planning a tool path for a large lap tool, and the inner part of the full-aperture surface error is corrected with weak mid-spatial frequency. The small lap is then introduced to correct the surface error in the edge-area of the optics. By this method, the mid-spatial-frequency surface error is effectively restrained, and the time consumption of optical fabrication is controlled.

Further simulations and experiments for a large off-axis SiC aspherical mirror indicate that the PV and RMS converge from initial values of 34.75 μm and 4.4 μm to 13.68 μm and 1.94 μm respectively, and the mid-spatial frequency is controlled effectively, which is favorable for the post-manufacturing process. This demonstrates the validity of the optimized combination strategy, which ensures high manufacturing efficiency while simultaneously improving surface accuracy. Generally, the strategy developed in this article could be widely applied to CCOS in both grinding and polishing processes.

Funding

National Natural Science Foundation of China (NSFC) (11903035, 11803037).

CRediT authorship contribution statement

Longxiang Li: Conceptualization, Formal analysis, Funding acquisition, Investigation, Writing - original draft. **Xingchang Li:** Data curation, Software. **Qiang Cheng:** Methodology. **Ruigang Li:** Project administration. **Weijie Deng:** Validation. **Xiao Luo:** Resources. **Feng Zhang:** Visualization. **Donglin Xue:** Writing - review & editing. **Xuejun Zhang:** Conceptualization, Supervision.

Declaration of Competing Interest

The authors declare that they have no known competing financial interests or personal relationships that could have appeared to influence the work reported in this paper.

References

[1] Kim DW, Kim SW, Burge JH. Non-sequential optimization technique for a computer controlled optical surfacing process using multiple tool influence functions. Opt Express 2009;17:21850–66.
[2] Del HJ, Heejoo C, Burge JH, Geon-Hee K, Wook KD. Experimental power spectral density analysis for mid- to high-spatial frequency surface error control. Appl Opt 2017;56:5258.
[3] Sidpara A. Magnetorheological finishing: a perfect solution to nanofinishing requirements. Opt Eng 2014;53:092002.
[4] Kheradmand S, Esmailian M, Fatahy A. A novel approach of magnetorheological abrasive fluid finishing with swirling-assisted inlet flow. Results Phys 2016;6(C):568–80.
[5] Beier M, Scheiding S, Gebhardt A, Loose R, Risse S, Eberhardt R, et al. Fabrication of high precision metallic freeform mirrors with magnetorheological finishing (MRF). Proc SPIE 2013;8884:88840S.
[6] Żak Andrzej, Łaszcz Amadeusz, Hasiak Mariusz. Gregory Gerstein, Hans Jürgen Maier, Wlodzimierz Dudzinskic. “Ion polishing as a method of imaging the magnetic structures in CoNiGa monocrystal. Result Phys 2018;6(C):277–80.
[7] Arnold T, Pietag F. Ion beam figuring machine for ultra-precision silicon spheres correction. Precis Eng 2015;41:119–25.
[8] Wang T, Huang L, Vescovi M, Kuhne D, Tayabaly K, Bouet N, et al. Study on an effective one-dimensional ion-beam figuring method. Opt Express 2019;27(11):15368–81.
[9] Wang T, Huang L, Kang H, Choi H, Kim DW, Tayabaly K, et al. RIFTA: A Robust Iterative Fourier Transform-based dwell time Algorithm for ultra-precision ion beam figuring of synchrotron mirrors. Sci Rep 2020;10(1):1–12.
[10] Hang D, Ci S, Shengyi L, Mingjin X, Xiaoqiang P. Optimization technique for rolled edge control process based on the acentric tool influence functions. Appl Opt 2017;56:4330.
[11] Forbes GW. Never-ending struggles with mid-spatial frequencies. SPIE Optical Metrology 2015.
[12] Nam HS, Kim GC, Kim HS, Rhee HG, Ghim YS. Modeling of edge tool influence functions for computer controlled optical surfacing process. Int J Adv Manuf Technol. 83. p. 911–17.
[13] Liu Z, Li L, Zeng X, Luo X, Zhang X. Fabrication of large aspheric mirror using multi-mode polishing based on error separation. Opt Precis Eng 2017;25(4):281–7.
[14] Jones RA. Fabrication of off-axis optical segments. Proc SPIE 1992;1752:73–82.
[15] Subrahmanyan P, Gardopee G, Verma Y, Ning L, Yu T, Kyler T, et al. Rapid fabrication of lightweight SiC aspheres using reactive atom plasma (RAPTM) processing. Proc. SPIE 2007.
[16] Li L, Xue D, Deng W, Wang X, Zhang X. Positive dwell time algorithm with minimum equal extra material removal in deterministic optical surfacing technology. Appl Opt 2017;56:9098.
[17] Li L, Hu H, Zheng L, Deng W, Xu W. “Optimized dwell time algorithm in magnetorheological finishing”Int. J. Adv. Manuf. Technol. 2015;81:833–41.
[18] Li L, Liu Z, Xue D, Deng W, Li R, Bai Y, et al. Rapid fabrication of a lightweight 2m reaction-bonded SiC aspherical mirror. Results Phys 2018;10:903–12.
[19] Wilson SR, McNeil JR. Neutral ion beam figuring of large optical surfaces. Proc. SPIE 1987;818:320–4.
[20] Drueding TW, Bifano TG, Fawcett SC. Contouring algorithm for ion figuring. Precis Eng 1995;17:10–21.
[21] Sandri G, Horenstein MN, Feinberg MR, Shanbhag PM, Bifano TG. Ion-beam machining of millimeter scale optics. Appl Opt 2000;39:599–611.
[22] Wilson S, McNeil J. Neutral ion beam figuring of large optical surfaces. 31st Annual Technical Symposium (International Society for Optics and Photonics). 1987. p. 320–4.
[23] Deng W, Zheng L, Shi Y, Wang X, Zhang X. Dwell time algorithm based on matrix algebra and regularization method. Opt Precis Eng 2007;15(7):1009–15. in Chinese.
[24] Luo X, Zheng L, Zhang X. Finite element analysis simulation and experimental verification of the stressed lap’s deformation accuracy. Appl Opt 2011;50(4):782.